Phys. Status Solidi B **246**, No. 5, 1072–1081 (2009) / **DOI** 10.1002/pssb.200844359

physica status solidi b
www.pss-b.com
basic solid state physics

Optical properties of pure and transition metal-doped indium oxide

H. A. Rahnamaye Aliabad[1,2], S. M. Hosseini[*,1], A. Kompany[1], A. Youssefi[3], and E. Attaran Kakhki[1]

[1] Department of Physics (Materials and Electroceramics Laboratory), Ferdowsi University of Mashhad, Iran
[2] Department of Physics, Tarbiat Moallem University of Sabzevar, Iran
[3] Par-E-Tavous Research Institute, Mashhad, Iran

Received 4 September 2008, revised 1 November 2008, accepted 28 November 2008
Published online 28 January 2009

PACS 71.15.Mb, 71.55.Gs, 78.20.Bh

[*] Corresponding author: e-mail sma_hosseini@yahoo.com, Phone: +98511 8435723, Fax: +98511 8796416

The band structure, the dielectric function, the reflectivity, the refractive index and the oscillator strength sum rule were calculated for pure In_2O_3 and alloyed $In_{1.5}T_{0.5}O_3$ (where T represents Sc, Y, La and Ac) using density functional theory (DFT). The full potential linearized augmented plane wave (FP-LAPW) method was used with the local density approximation (LDA + *U*). Calculations of the optical spectra were performed for the energy range 0–30 eV. The calculated results indicate that the upper valance bands of In_2O_3 show a small dispersion and the value of the band gap increases for Sc and Y dopants and decreases for Ac and La dopants. The calculations indicate that there are two band gaps for In_2O_3. The first shows a strong optical absorption, as a direct band gap occurs from a 0.81 eV energy level below the top of valence band. The second shows a much weaker absorption from the top of the valence band to the bottom of the conduction band. The refractive index for In_2O_3 is 1.69 nm at 800 nm, near the visible region.

1 Introduction Transparent conducting oxides (TCOs) such as In_2O_3, SnO_2, ZnO and CdO are n-type wide band-gap semiconductor materials. Thin films of these materials have been prepared by various methods and widely used practically in optoelectronic devices, as transparent electrodes in panel displays, in thin-film transistors and in infrared reflectors [1–3]. They exhibit high transmittance in the visible and near-infrared regions. The electrical and optical properties of these materials can be altered by introducing impurities. The properties of doped TCO films are very sensitive to the type of impurities. It is also interesting to study the alloys of these materials to see how the structure and properties are affected when the composition changes [4]. For example, indium oxide doped with tin (ITO) acts as a metal-like material due to the high density of free electrons in the conduction band and can be used as a good spectral-selective surface for solar collectors [5]. Recently, a novel transparent conductive film, molybdenum-doped indium oxide, with mobility twice that of TCO materials, has been developed [6–9].

However, in order to obtain optimal characteristics, i.e. high transparency, optical transmission in the visible region and low sheet resistance, parameters such as dopant type and amount and other deposition conditions have to be optimized. There is a possibility to control the electronic and optical properties of In_2O_3 by doping it with transition metals, as the d states of these metals are very sensitive. Substituting indium atoms at b-positions (see Fig. 2) by group IIIB elements considerably increases the value of the band gap mainly due to the number of states originating from IIIB d states in the conduction band [4, 10]. Medvedeva [11] has demonstrated that the advantages of transition metal (Mo) doping are a smaller effective mass, larger fundamental band gap and better overall optical transmission in the visible region, as compared to commercial Sn-doped In_2O_3. In this article we report first-principles electrical and optical properties investigations of the effect of Sc, Y, La and Ac substitutions on various parameters of indium oxide: band gap, dielectric function, absorption coefficient, reflectivity, refractive index and the oscillator strength sum rule.

2 Method of calculation The calculations were carried out with a self-consistent scheme by solving the

Kohn–Sham equations using the full potential linearized augmented plane wave (FP-LAPW) method in the framework of density functional theory (DFT) along with the local density approximation (LDA) [12, 13] using Wien2k codes [14]. The calculation was performed with 1728 ($12 \times 12 \times 12$) k-points and $Rk_{max} = 6$ (where R is the smallest muffin-tin radius and k_{max} is the cut-off for the plane wave) for the convergence parameter for which the calculations stabilize and converge in terms of the desired charge. The value of $G_{max} = 12$ (the magnitude of largest vector in charge density Fourier expansion or the plane wave cut-off) and the muffin-tin radii for In and O were R_{MT} (In) = 2.0 a.u. and R_{MT} (O) = 1.6 a.u., respectively. The iteration was halted when the charge difference was less than $0.001e$ between steps as the convergence criterion. The cut-off energy, which defines the separation of the valence and core states, was chosen as -7 Ry.

To calculate the electronic and optical properties of pure In_2O_3 and alloyed $In_{1.5}T_{0.5}O_3$ (where T represents Sc, Y, La and Ac), we considered the interaction of d-localized valence electrons, due to the presence of their spins. This might be the reason for the smaller band gap obtained for In_2O_3 using the LDA or generalized gradient approximation (GGA) compared to the experimental values. In order to calculate the electronic properties of In_2O_3 using LDA + U, we assumed that the density matrix is diagonal and U is the same for all Coulomb interactions ($U_{ij} \equiv U$) and J is also the same for all exchange interactions ($J_{ij} \equiv J$).

There are several methods to incorporate the U-term [15, 16], but here we used the self-interaction correction (SIC) introduced by Anisimov and co-workers [17] as implemented in the Wien2k package. In the LDA + U^{SIC} methods, the total energy may be written as

$$E = E_0 + E_{\mathrm{LDA}+U^{\mathrm{SIC}}}, \tag{1}$$

where

$$E_{\mathrm{LDA}+U^{\mathrm{SIC}}} = \frac{U-J}{2}\left(N - \sum_{m,\sigma} n_{m,\sigma}^2\right), \tag{2}$$

in which N is the total number of electrons and $n_{m,\sigma}$ is the orbital occupancy of the ℓ-orbital in question (i.e. s, p or d orbital) with spin σ. With an approximated correction value of $U - J$ for the SIC, this is probably best for a strongly correlated system and for a full potential method.

If the uncorrected LDA functional is used ($U_{eff} = 0$ eV), the In 4d band in the density of states is located at significantly lower binding energies compared to experiments, as shown in Fig. 1. Increasing U_{eff} affects the position of the deep In 4d-dominated band most prominently, which is shifted to more negative binding energies. The Hubbard potential used in this work was $U_{eff} = U - J = 8.98$ eV for the In atom. We used this value of U in order to adjust the In 4d orbital level with the experimental value of about 15 eV [18].

The calculations were first carried out by applying the experimental data for the lattice constants. Then by minimizing the total energy of the crystal to the volume, the theoretical lattice constants were obtained. We substituted the impurities in b-positions (see Fig. 2) since at low temperatures the impurities prefer to sit at b-positions [11]. The final calculation was performed with the theoretical lattice constant and relaxed structure for In_2O_3 and $In_{1.5}T_{0.5}O_3$.

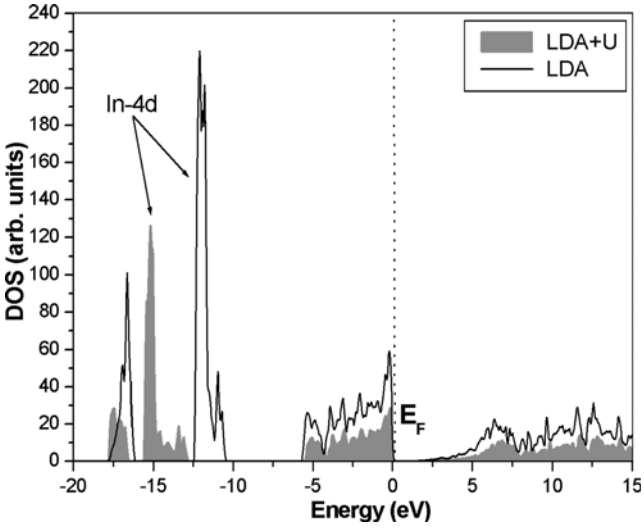

Figure 1 Calculated total density of states (DOS) of In_2O_3 using LDA and LDA + U.

3 Structure Indium oxide can exist in three different phases characterized by space group symmetries $I2_13$, $Ia\bar{3}$ and $R\bar{3}$ [19]. In_2O_3 with space group $Ia\bar{3}$ and band gap of $E_g = 3.7$ eV is similar to many trivalent rare earth oxides, such as Yb_2O_3 and Dy_2O_3. This phase of indium oxide has two non-equivalent six-fold-coordinated cation sites, as shown in Fig. 2. Its structure is cubic and the optical spectra are isotropic along the crystallographic a-, b- and

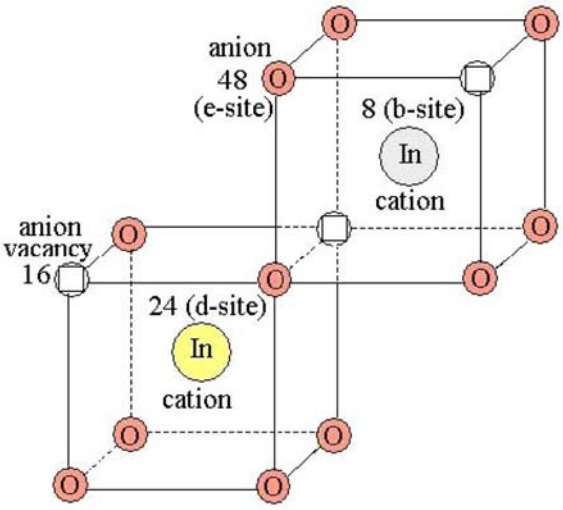

Figure 2 (online colour at: www.pss-b.com) Non-equivalent cation sites and anion vacancies in In_2O_3.

c-axis, i.e. there is only one independent component. The two non-equivalent cation sites are referred to as equipoints 'b' and 'd'. The b-site cations have six equidistant oxygen anion neighbours, which lie approximately at the corners of a cube with two anion structural vacancies along one body diagonal [20]. The sites of the cations are coordinated to six oxygen anions at three different distances, which lie near the corners of a distorted cube with two empty ions along one face diagonal. The unit cell contains 80 atoms and crystallizes in a cubic bixbyite structure. The actual unit cell is body-centred and contains 8 formula units of In_2O_3 with 8 indium atoms at b-positions, 24 atoms at d-positions and 48 oxygen atoms at e-positions.

4 Results and discussion

4.1 Total energy In terms of energy, the bulk modulus is also defined by equation of states (EOS). The position of the minimum of the EOS defines the equilibrium lattice parameter and unit cell volume at zero pressure. The static lattice potential corresponding to total energy was calculated from a series of strained lattices. From such results the equilibrium volume, bulk modulus and its pressure derivative were derived. A series of total energy calculations as a function of volume can be fitted to an EOS according to Murnaghan [21]:

$$E(V) = E_0 + \frac{B_0 V}{B_0'}\left[\frac{(V_0/V)^{B_0'}}{B_0'} + 1\right] - \frac{B_0 V_0}{B_0' - 1}, \qquad (3)$$

where B_0 is an equilibrium bulk modulus that effectively measures the curvature of the energy versus volume curve about the relaxed volume V_0 and B_0' is the derivative of the bulk modulus.

We minimized the energy for atomic positions and determined the equilibrium position of individual atoms. The final calculation was performed with the theoretical lattice constant and relaxed structure. The results of minimum energy, E_0, equilibrium volume, V_0, bulk modulus, B, and derivative of the bulk modulus, B', are summarized in Table 1.

Table 1 Calculated equilibrium data for In_2O_3 and alloyed $In_{1.5}T_{0.5}O_3$.

compound	E_0 (eV)	V_0 (Å^3)	B (GPa)	B'
In_2O_3 (this work)	−14088.89	1017.20	186.64	5.64
In_2O_3 (LDA + U) [22]	–	–	180	4.6
In_2O_3 (GGA) [19]	–	1023.28	172.87	4.75
$In_{1.5}Sc_{0.5}O_3$	−11081.12	996.11	194.49	5.61
$In_{1.5}Y_{0.5}O_3$	−12621.29	1057.16	172.50	5.03
$In_{1.5}La_{0.5}O_3$	−15625.46	1139.86	152.26	4.48
$In_{1.5}Ac_{0.5}O_3$	−25786.74	1172.91	201.37	1.94

The calculated total energies of the structures with Ac and La atoms doping at the b-site are lower than that of pure In_2O_3 by 11697.55 and 1537.67 eV, but higher than those with Y and Sc atoms doping by 1467.60 eV and 3007.77 eV, respectively.

4.2 Band gaps We calculated the band gaps of pure In_2O_3 and alloyed $In_{1.5}T_{0.5}O_3$ from the band structure as shown in Fig. 3, using the LDA + U approach. The top of the valence band is set to zero as the Fermi level on the energy scale.

In Fig. 3 the first band gap E_g^a is the energy difference between the top of the valence band and the bottom of the conduction band in the Γ direction. The second band gap E_g^b is the energy difference between the two lowest minimum energies in the N direction.

Experimental measurements on In_2O_3 single crystals shows that there is a strong optical absorption with a direct band gap at an energy of 3.75 eV and a much weaker absorption at an energy of 2.62 eV [23]. According to the results of Walsh et al. [24] the strong optical transition can occur from Γ_1 to Γ_3 as a direct band gap. The weaker absorption is from Γ_2 to Γ_3 as an indirect band gap. In fact the direct optical transitions at Γ from the valence band maxi-

Table 2 Calculated band gap values for In_2O_3 and alloyed $In_{1.5}T_{0.5}O_3$.

band gap (eV)	E_g^a	E_g^b	$\Gamma_1 \rightarrow \Gamma_2$	$\Gamma_2 \rightarrow \Gamma_3$ (indirect)	$\Gamma_1 \rightarrow \Gamma_3$ (direct)
this work (FP-LAPW method with GGA + U)					
In_2O_3	1.43	2.04	0.78	1.43	2.21
$In_{1.5}Sc_{0.5}O_3$	2.18	1.68	–	–	–
$In_{1.5}Y_{0.5}O_3$	1.88	176	–	–	–
$In_{1.5}La_{0.5}O_3$	1.24	1.76	–	–	–
$In_{1.5}Ac_{0.5}O_3$	0.82	1.80	–	–	–
theory					
In_2O_3 (LDA) [19]	1.10	2.86	–	–	–
In_2O_3 (GGA) [4]	1.03	1.77	–	–	–
In_2O_3 (LMTO) [25]	1.0	–	–	–	–
experimental					
In_2O_3 thin film [26]	–	–	–	–	3.27
In_2O_3 thin film [27]	–	–	–	2.1 ± 0.2	3.5 ± 0.1
In_2O_3 bulk [23, 24]	–	–	0.82	2.62	3.75

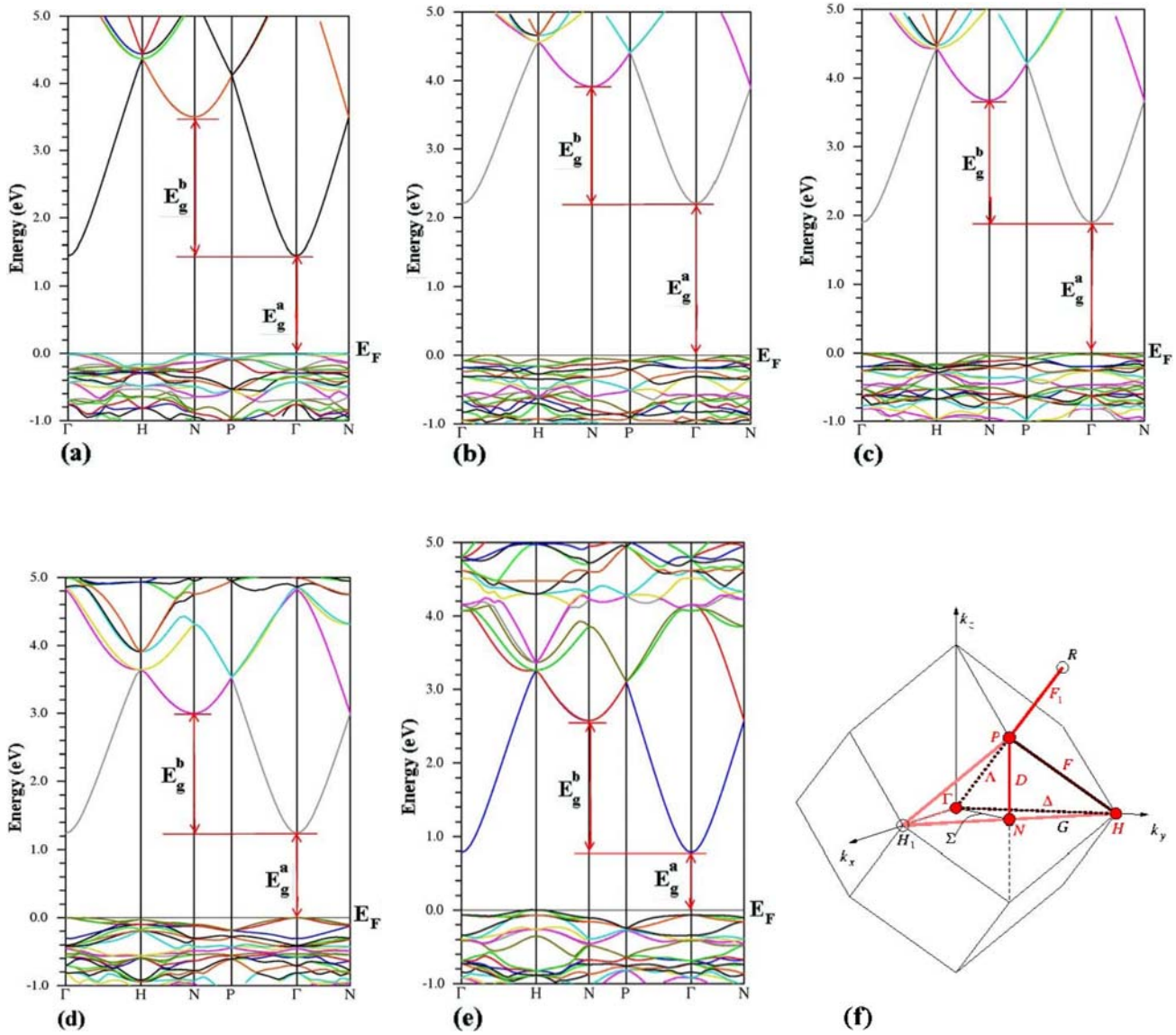

Figure 3 (online colour at: www.pss-b.com) Calculated band structures of a) In_2O_3, b) $In_{1.5}Sc_{0.5}O_3$, c) $In_{1.5}Y_{0.5}O_3$, d) $In_{1.5}La_{0.5}O_3$ and e) $In_{1.5}Ac_{0.5}O_3$. f) Selected directions in the primitive Brillouin zone.

Table 3 High-frequency dielectric constants, $\varepsilon(\infty)$, of pure In_2O_3 and alloyed $In_{1.5}T_{0.5}O_3$.

method	In_2O_3	$In_{1.5}Sc_{0.5}O_3$	$In_{1.5}Y_{0.5}O_3$	$In_{1.5}La_{0.5}O_3$	$In_{1.5}Ac_{0.5}O_3$
experimental					
thin film [29]	3.62	–	–	–	–
theoretical					
Ref. [19][a]	4.54	–	–	–	–
Ref. [30][b]	3.82	–	–	–	–
this work (without scissors operator)	2.69	2.58	2.60	2.78	3.06

[a] Shifted towards lower energies compared with experimental results.
[b] Calculated in the independent quasiparticle using the approach to compensate the gap underestimation found in the LDA.

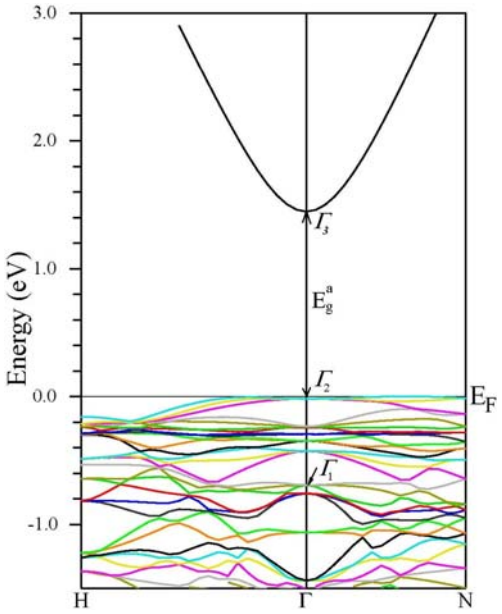

Figure 4 (online colour at: www.pss-b.com) Portion of the band structure for In_2O_3.

mum (VBM) to the conduction band minimum (CBM) are parity forbidden and the first strong transitions occur from valence bands 0.81 eV below the VBM. In Fig. 4 a portion of the calculated band structure of In_2O_3 shows that the upper valence bands of In_2O_3 exhibit a small dispersion and the CBM is positioned at point Γ_3. This band gap discrepancy is consistent with the results reported by Walsh et al. [24].

The calculated values of these band gaps are summarized in Table 2. The value of E_g^a increases with Sc and Y doping due to a decrease in the lattice parameter, while with La and Ac it decreases mainly due to an increase in the lattice parameter. It can be seen from Table 2 that the value of E_g^a is reduced for all the dopants compared to the band gap of pure In_2O_3 crystal.

Since the calculated result for the band gap by DFT gives an underestimate of the value, the band gaps calculated in this work are still smaller than the experimental values, but larger than some theoretical values. To solve this problem and obtain values close to the experimental ones, some workers have shifted the band structures rigidly to higher values, in order to adjust the band gap, by adding a constant to their values (scissors operation). However, for calculation of the optical properties we did not shift towards lower energies to increase the value of the band gap, and therefore the results appear, in this paper, smaller than the experimental values.

4.3 Dielectric function The imaginary part of the optical dielectric function can be derived from knowledge of the electronic band structure of a solid by summing interband transitions from occupied to unoccupied states for energies much higher than phonons. It is well known that the interaction of a photon with the electrons in a system can be described in terms of time-dependent perturbations of the ground state of the electronic states. Transitions between occupied and unoccupied states, including plasmons and single-particle excitations, are caused by the electric field of the photon.

The spectra resulting from these excitations can be described as a joint density of states between the valence and conduction bands. The dielectric function $\varepsilon(\omega)$, which describes the features of the linear response of the system to electromagnetic radiation, actually governs the propagation behaviour of radiation in a medium. Generally, $\varepsilon(\omega)$ is connected with the interaction of photons with electrons. However, we have used the random phase approximation (RPA) approach for the calculation of the imaginary part of dielectric function for pure In_2O_3 and alloyed $In_{1.5}T_{0.5}O_3$ as implemented in Wien2k codes [28]. The real part is obtained using the Kramers–Kronig transformation.

The real and the imaginary parts of the frequency-dependent dielectric function for pure In_2O_3 and alloyed

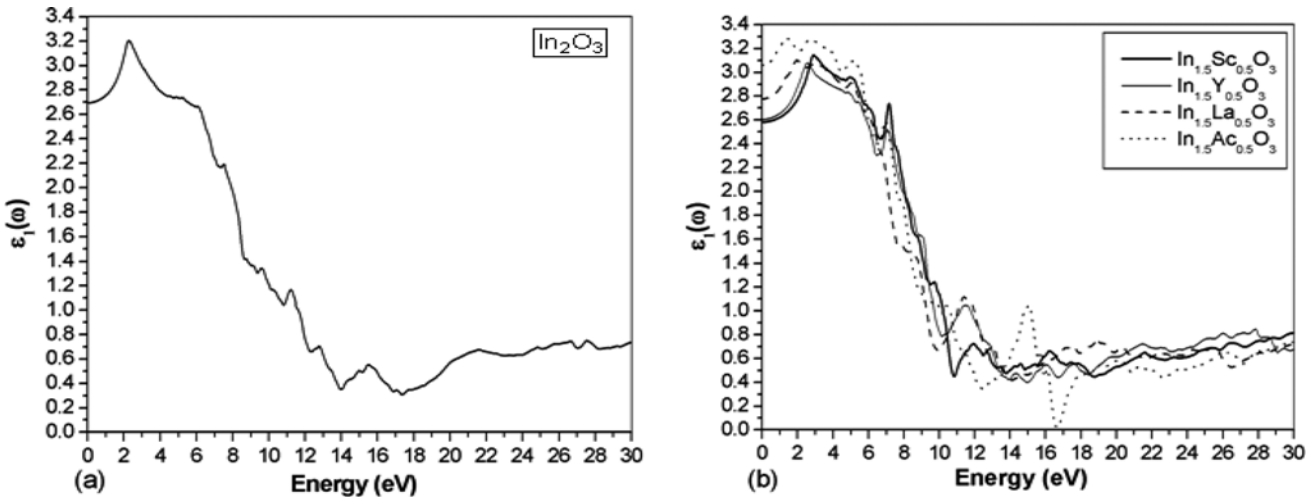

Figure 5 Real part of the dielectric function for a) In_2O_3 and b) $In_{1.5}T_{0.5}O_3$.

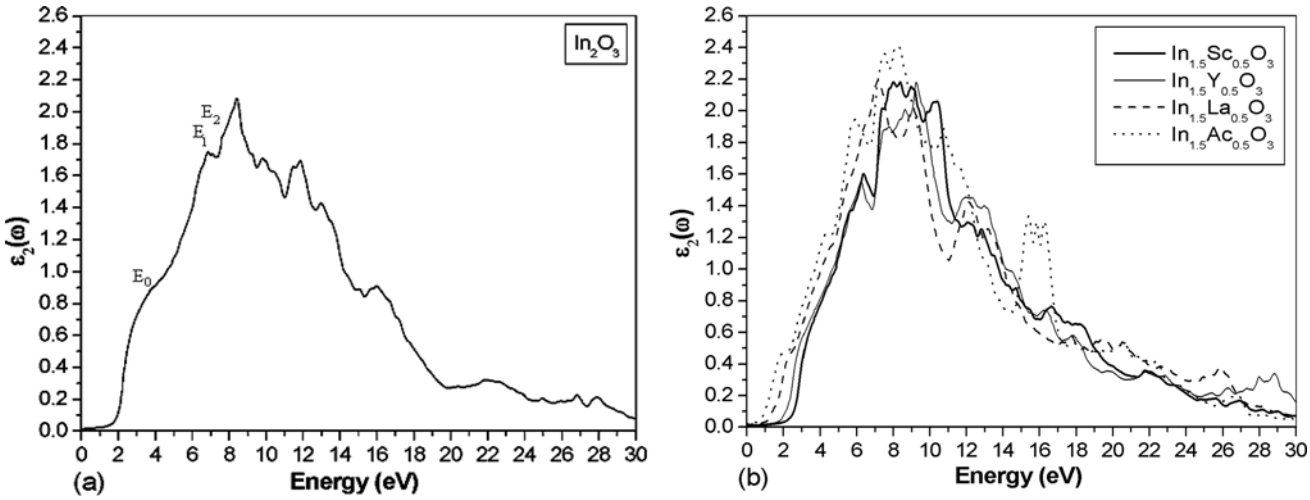

Figure 6 Imaginary part of the dielectric function for a) In_2O_3 and b) $In_{1.5}T_{0.5}O_3$.

$In_{1.5}T_{0.5}O_3$ are shown in Figs. 5 and 6. The static dielectric permittivity tensor, $\varepsilon_{\alpha\beta}(0)$, of a nonpolar material contains electronic (high-frequency) and ionic contribution. The high-frequency dielectric constants, $\varepsilon(\infty)$, of pure In_2O_3 and alloyed $In_{1.5}T_{0.5}O_3$ are presented in Table 3.

Again, we did not shift towards lower energies to increase the value of the band gap, and therefore the results for the high-frequency dielectric constant that appear in this work are smaller than values reported by others.

The calculated Im $\varepsilon(\omega)$ (Fig. 6) shows the first peak at about $E_0 = 2.35$ eV which is due to the fundamental gap. This peak is related to the interband transition from the valence to the conduction band states at the Γ-point. For simplification of the analysis of the other optical transition spectra, the labels E_0, E_1 and E_2 have been used. Subscript 0 refers to transitions at point in [000] along the Γ direction, 1 to transitions at point in [111] along the Γ–P direction and 2 to transitions at [100] along direction Γ–H of ***k***-space. These notations are used based on those of Ref. [31] to describe the reflectivity spectra of semiconductors of wurtzite and zinc blend structures.

4.4 Reflectivity Figure 7 shows the calculated reflectivity spectra for In_2O_3 and alloyed $In_{1.5}T_{0.5}O_3$ for the energy range 0–30 eV.

We compare the calculated reflectivity of In_2O_3 with experimental measured optical spectra as shown in Fig. 7a for a short energy range of 2.5–4 eV from Ref. [32]. The calculated results for this energy range are in good agreement with experimental data.

However, at higher energies well above the band gap and at lower energies near the band gap, the experimental

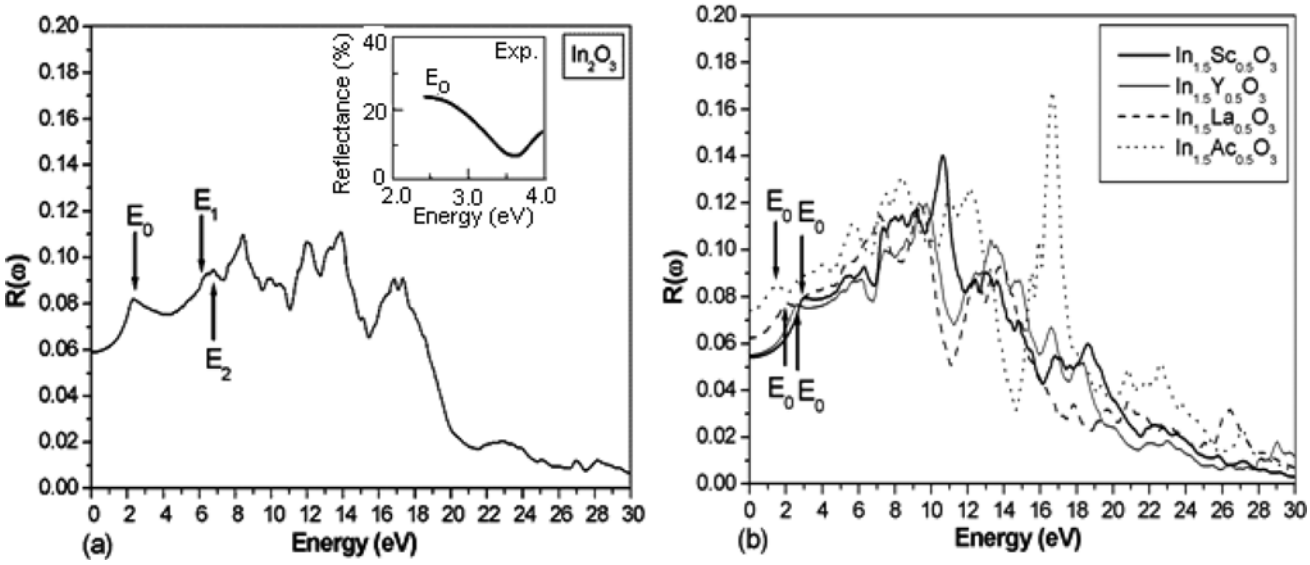

Figure 7 Reflectivity as function of the photon energy for a) In_2O_3 and b) $In_{1.5}T_{0.5}O_3$. The inset in a) is from Ref. [32].

Table 4 Peak values of the reflectivity for In_2O_3 and $In_{1.5}T_{0.5}O_3$.

compound	E_0 (eV)	E_1 (eV)	E_2 (eV)
this work (FP-LAPW method with GGA + U)			
In_2O_3	2.35	6.16	6.79
$In_{1.5}Sc_{0.5}O_3$	3.44	5.54	6.35
$In_{1.5}Y_{0.5}O_3$	2.87	5.21	5.67
$In_{1.5}La_{0.5}O_3$	2.05	3.69	4.50
$In_{1.5}Ac_{0.5}O_3$	1.59	2.90	4.01
theory			
In_2O_3 (DFT, FP-LAPW) [19][a]	2.24	6.13	7.24
experimental			
In_2O_3 [34][b]	2.42	–	–

[a] Shifted towards lower energies compared with experimental results.
[b] Films of pure and Sn-doped indium oxide were prepared by reactive e-beam evaporation.

reflectivity is higher than that calculated in this work. The experimentally observed low-energy peak may be associated with an excitonic effect which has not been considered in the present calculations. We can also conclude that In_2O_3 is a transparent material in the visible region.

The positions of three peaks in the reflectivity spectra calculated in this work are summarized in Table 4.

4.5 Refractive index and dispersion The wavelength dependency of a material's refractive index is usually quantified by an empirical formula, the Cauchy or Sellmeier equations. In this work we only present the calculated wavelength dispersion of refractive index for In_2O_3 and $In_{1.5}T_{0.5}O_3$, as shown in Fig. 8.

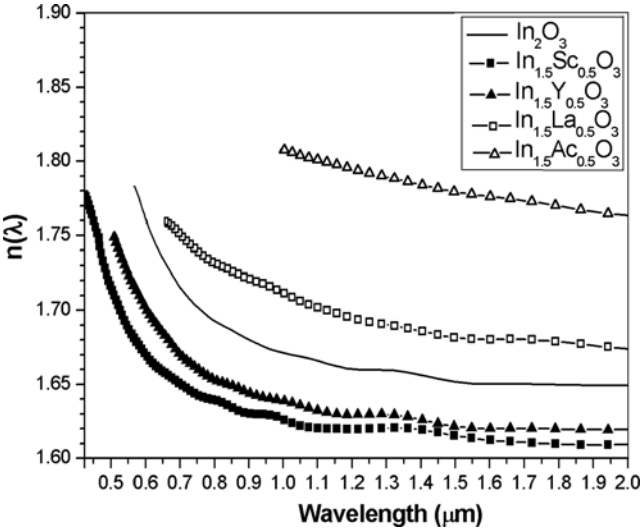

Figure 8 Refractive index (n) as function of wavelength for In_2O_3 and $In_{1.5}T_{0.5}O_3$.

The curves are fairly flat in the long-wavelength region and rise rapidly at shorter wavelengths, showing the typical shape of the dispersion curve near an electronic interband transition.

The calculated refractive indices of the structures with Ac and La atoms are higher than that of pure In_2O_3, but lower than those with Y and Sc atoms. The calculated and experimental values of refractive index at various wavelengths are summarized in Table 5.

Table 5 Refractive index (n) for selected wavelengths for In_2O_3 and $In_{1.5}T_{0.5}O_3$.

compound	0.5 μm	0.6 μm	0.7 μm	0.8 μm	0.9 μm	1.0 μm
this work						
In_2O_3	1.78	1.76	1.71	1.69	1.68	1.67
$In_{1.5}Sc_{0.5}O_3$	1.71	1.67	1.65	1.64	1.63	1.63
$In_{1.5}Y_{0.5}O_3$	1.75	1.70	1.67	1.65	1.64	1.64
$In_{1.5}La_{0.5}O_3$	–	–	1.75	1.73	1.72	1.71
$In_{1.5}Ac_{0.5}O_3$	–	–	–	–	–	1.81
theory						
In_2O_3 [19][a]	2.13	–	–	–	–	–
experimental						
In_2O_3 [33][b]	1.90	1.71	1.71	1.66	1.64	1.69
In_2O_3 [29][b]	1.93	1.90	1.88	1.85	1.84	1.83
In_2O_3 [32][c]	2.02	–	–	–	–	–
ITO [32][c]	1.91	–	–	–	–	–
ITO [34][d]	2.08	2.0	1.98	1.97	1.95	1.93
ITO [35][e]	1.88	1.65	1.61	1.61	1.61	1.61

[a] Theoretical; DFT, FP-LAPW.
[b] Experimental; thin films of indium oxide were deposited using the chemical spray pyrolysis technique at 400 °C.
[c] Experimental; films of pure and Sn-doped indium oxide were prepared by reactive e-beam evaporation.
[d] Experimental; a metal alloy target of indium doped with tin was radiofrequency-sputtered in oxygen onto quartz substrates (annealed at 200 °C).
[e] ITO thin films (In_2O_3 : SnO_2) were prepared using the sol–gel dip-coating process on glass substrates.

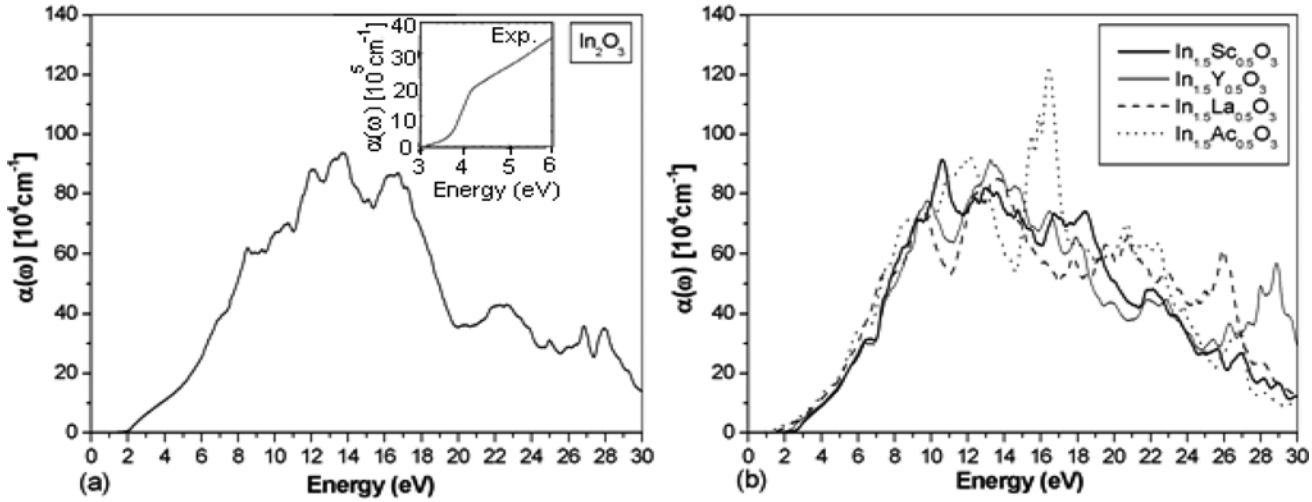

Figure 9 Absorption coefficients as a function of photon energy for a) In_2O_3 and b) $In_{1.5}T_{0.5}O_3$. The inset in a) is from Ref. [32].

4.6 Absorption We used the following relation for calculating absorption:

$$\alpha_{\alpha\beta}(\omega) = \frac{2\omega k_{\alpha\beta}(\omega)}{c}. \tag{4}$$

Figure 9 shows the calculated absorption for pure In_2O_3 and $In_{1.5}T_{0.5}O_3$. The absorption coefficient $\alpha(\omega)$ is very large (about 10^6 cm^{-1}) and decreases rapidly in the low-energy region. In the visible range, $\alpha(\omega)$ is equal to zero, meaning that the material for visible wavelengths is transparent. The calculated absorption spectra agree with the measured spectra at lower energies [32]. However, at energies exceeding the location of the E_0 peak, the calculated absorption coefficient is found to be much smaller than that determined experimentally.

4.7 Oscillator strength sum rule Another way to consider the number of electrons involved in the valance interband transition is to evaluate the sum rule. The effective number of valance electrons per atom, n_{eff}, contributing to a transition up to finite frequency range is given by the following relation [36]:

$$\int_0^{\omega} \omega\varepsilon_2(\omega)\,\mathrm{d}\omega = \frac{1}{2}\pi\left(\frac{4\pi N_a e^2}{m}\right) n_{\text{eff}}(\omega_c), \tag{5}$$

where N_a is the density of atoms per formula unit.

We calculated the oscillator strength sum rule for In_2O_3 and alloyed $In_{1.5}T_{0.5}O_3$ using the following equation [28]:

$$\int_0^{\omega'} \mathrm{Im}\left(\frac{-1}{\varepsilon(\omega)}\right)\omega\,\mathrm{d}\omega = N_{\text{eff}}, \tag{6}$$

where N_{eff} is the effective number of valence electrons for each formula unit f In_2O_3.

The results for the sum rule for pure In_2O_3 and alloyed $In_{1.5}T_{0.5}O_3$ are shown in Fig. 10. The value of N_{eff} is zero at low energy then rises rapidly and saturates at about 28 eV, with a value of 35.5 for In_2O_3.

For all sum rule curves, there is a break in the curves before saturation, which may be related to the onset of d-band excitations. Similar behaviour has been observed in III–V semiconductor compounds (i.e. GaAs, GaP and InSb) [37].

The sum rule does not saturate below an energy of 25 eV, which means that interband transitions play an important role in the optical properties of these materials. The effective number of valence electrons depends on the energy range contributing to a transition up to finite frequency range.

The effective number of electrons as a function of the band gap is shown in Fig. 11. The effective number of electrons increases with increasing band gap.

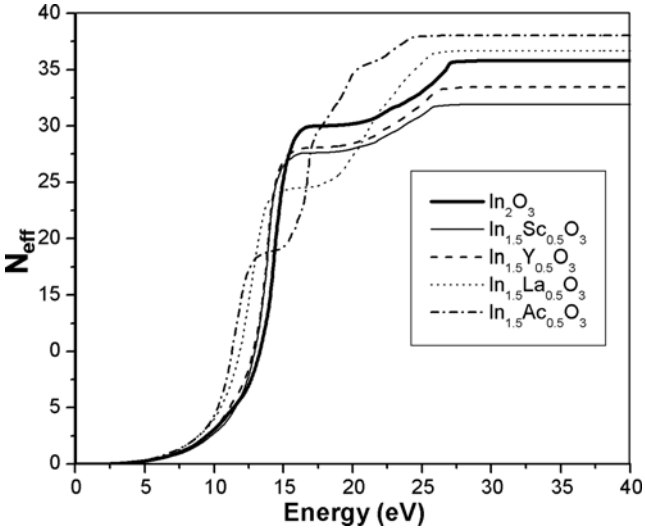

Figure 10 Oscillator strength sum rule as a function of photon energy for In_2O_3 and $In_{1.5}T_{0.5}O_3$.

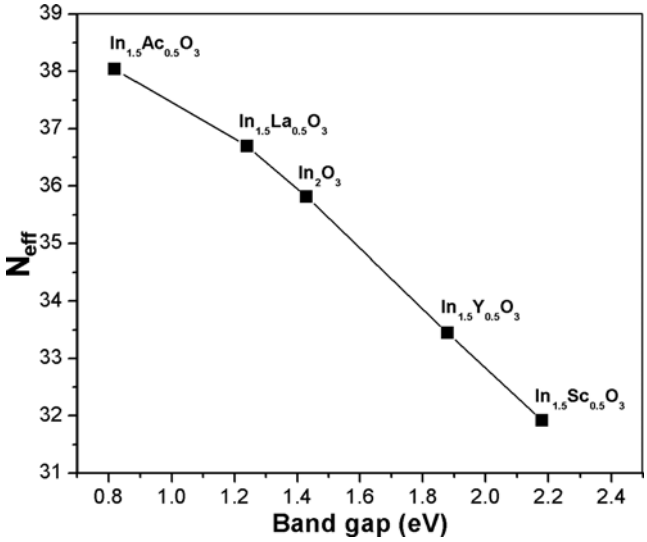

Figure 11 Effective number of electrons as a function of the band gap for In_2O_3 and $In_{1.5}T_{0.5}O_3$.

The effective number of electrons that contribute in the transition, the energy range for which the calculations were performed and the free valence electrons are summarized in Table 6.

4.8 Electron energy loss spectroscopy (EELS) EELS is a valuable tool for investigating various aspects of materials [38]. It has the advantage of covering the complete energy range including non-scattered and elastically scattered electrons (zero loss), electrons that excite an atom's outer shell (valence loss) or valence interband transitions. Also the fast electrons excite the inner shell electrons (core loss) or induce core level excitation of nearedge structure (ELNES) and XANES. In the case of interband transitions, this consists mostly of plasmon excitations. The scattering probability for volume losses is directly

Table 6 Calculated plasmon energy $\hbar\omega_p$ for In_2O_3 and alloyed $In_{1.5}T_{0.5}O_3$.

compound	N_{eff}	energy range (eV)	plasmon energy, $\hbar\omega_p$ (eV)
In_2O_3	35.808	(−17)–11	14.29
$In_{1.5}Sc_{0.5}O_3$	31.919	(−17)–11	14.14
$In_{1.5}Y_{0.5}O_3$	33.446	(−17)–11	13.86
$In_{1.5}La_{0.5}O_3$	36.696	(−17)–11	12.78
$In_{1.5}Ac_{0.5}O_3$	38.033	(−17)–11	11.36

connected to the energy loss function. One can then calculate the EEL spectrum from the following relations [28]:

$$\varepsilon_{\alpha\beta}(\omega) = \varepsilon_1 + i\varepsilon_2$$

and

$$\text{EEL spectrum} = \text{Im}\left(\frac{-1}{\varepsilon_{\alpha\beta}(\omega)}\right) = \frac{\varepsilon_2}{\varepsilon_1^2 + \varepsilon_2^2}. \quad (7)$$

In Fig. 12 the energy loss function is plotted for In_2O_3 and alloyed $In_{1.5}T_{0.5}O_3$ in the energy range 0–30 eV. The energy of the main maximum of Im $[-\varepsilon^{-1}(E)]$ is assigned to the energy of volume plasmon $\hbar\omega_p$. The values of $\hbar\omega_p$ obtained in this work are given in Table 6.

5 Conclusions The optical properties of pure In_2O_3 and alloyed $In_{1.5}T_{0.5}O_3$ have been calculated using DFT. Calculations of the optical spectra have been performed in the energy range 0–30 eV. Doping In_2O_3 with Sc and Y causes an increase in the band gap while with Ac and La dopants it decreases. The calculated high-frequency dielectric constant, $\varepsilon(\infty)$, without scissors operation, is equal to 2.69 for pure In_2O_3. The calculated Im $\varepsilon(\omega)$ shows a first peak at about $E_0 = 2.35$ eV and this is related to the interband transition from the valence to the conduction band

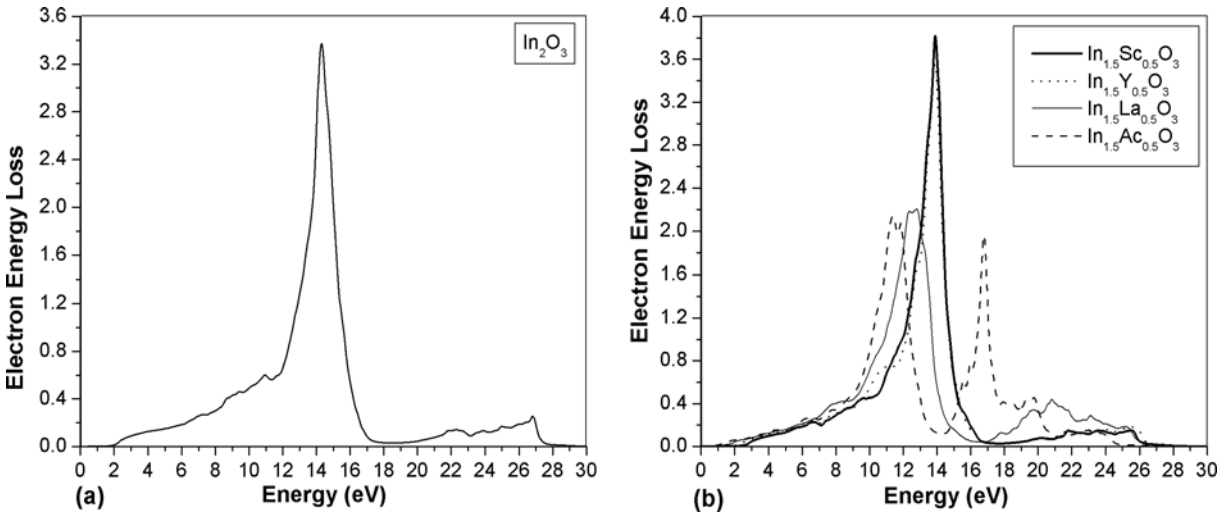

Figure 12 Electron energy loss for a) In_2O_3 and b) $In_{1.5}T_{0.5}O_3$.

states at the Γ-point. It is shown that the material is transparent at visible wavelengths and the dispersion curve of refractive index is fairly flat in the long-wavelength region and rises rapidly towards shorter wavelengths. The refractive index is 1.69 nm at 800 nm near the visible region. The effective number of valence electrons saturates at about 28 eV, with a value of 35.5 for In_2O_3. For all sum rule curves, there is a break in the curves before saturation which can be related to the onset of d-band excitations. The calculated sum rule does not saturate below an energy of 25 eV. This means that the interband transitions play an important role in the optical properties of these materials.

Acknowledgement The authors are grateful to Professor P. Blaha (at Vienna University of Technology, Austria) for his technical assistance in the use of Wien2k codes.

References

[1] D. S. Ginley, M. P. Taylor, M. F. A. M. van Hest, D. Young, C. W. Teplin, J. L. Alleman, M. S. Dabney, P. Parilla, L. M. Gedvilas, B. M. Keyes, B. To, D. Readey, and J. D. Perkins, Combinatorial Exploration of Novel Transparent Conducting Oxide Materials, Solar Energy Technologies Program Review Meeting, Denver, CO, 7–10 November 2005.
[2] P. Prathap, Y. P. V. Subbaiah, M. Devika, and K. T. Ramakrishna Reddy, Mater. Chem. Phys. **100**, 375 (2006).
[3] S. Laux, N. Kaiser, A. Zöller, R. Götzelmann, H. Lauth, and H. Bernitzki, Thin Solid Films **335**, 1 (1998).
[4] A. Kompany, H. A. Rahnamaye Aliabad, and S. M. Hosseini, Phys. Status Solidi B **244**, 619 (2007).
[5] F. Simonis, M. van der Leij, and C. J. Hoogendoorn, Solar Energy Mater. **1**, 221 (1979).
[6] Y. Meng, X. Yang, H. Chen, J. Shen, Y. Jiang, Z. Zhang, and Z. Hua, J. Vac. Sci. Technol. A **20**, 288 (2002).
[7] Y. Yoshida, T. A. Gessert, C. L. Perkins, and T. J. Coutts, J. Vac. Sci. Technol. A **21**, 1092 (2003).
[8] Y. Yoshida, D. M. Wood, T. A. Gessert, and T. J. Coutts, Appl. Phys. Lett. **84**, 2097 (2004).
[9] S. Sun, J. Huang, and D. Lii, J. Mater. Res. **20**, 247 (2005).
[10] A. Ambrosini, A. Duate, K. R. Poeppelmeier, M. Lane, C. R. Kannewurf, and T. O. Mason, J. Solid State Chem. **163**, 41 (2000).
[11] J. E. Medvedeva, Phys. Rev. Lett. **97**, 086401 (2006).
[12] J. P. Perdew, J. A. Chevary, S. H. Vosko, K. A. Jackson, M. R. Pederson, D. J. Singh, and C. Fiolhais, Phys. Rev. B **46**, 6671 (1992).
[13] M. Peterson, F. Wanger, L. Hufnagel, M. Scheffler, P. Blaha, and K. Schwarz, Comput. Phys. Commun. **126**, 294 (2000).
[14] P. Blaha, K. Schwarz, G. Madsen, D. Kvasnicka, and J. Luitz, Institute for Materials Chemistry, TU Vienna (http://www.wien2k.at/).
[15] A. G. Petukhov and I. I. Mazin, Phys. Rev. B **67**, 153106 (2003).
[16] P. Novak, J. Kunes, L. Chaput, and W. E. Pickett, Phys. Status Solidi B **243**, 563 (2006).
[17] V. I. Anisimov, I. V. Solovyev, M. A. Korotin, M. T. Czyzyk, and G. A. Sawatzky, Phys. Rev. B **48**, 16929 (1993).
[18] A. Klein, Appl. Phys. Lett. **77**, 2009 (2000).
[19] S. Zh. Karazhanov, P. Ravindran, P. Vajeeston, A. Ulyashin, T. G. Finstad, and H. Fjellvåg, Phys. Rev. B **76**, 075129 (2007).
[20] A. J. C. Wilson, The International Union of Crystallography, International Tables for Crystallography (Kluwer Academic, Dordrecht, 1992).
[21] F. D. Murnaghan, Proc. Natl. Acad. Sci. USA **30**, 244 (1944).
[22] P. Erhart, A. Klein, R. G. Egdell, and K. Albel, Phys. Rev. B **75**, 153205 (2007).
[23] R. L. Weiher and R. P. Ley, J. Appl. Phys. **37**, 299 (1966).
[24] A. Walsh, J. L. F. Da Silva, Su-Huai Wei, C. Körber, A. Klein, L. F. J. Piper, A. DeMasi, K. E. Smith, G. Panaccione, P. Torelli, D. J. Payne, A. Bourlange, and R. G. Egdell, Phys. Rev. Lett. **100**, 167402 (2008).
[25] H. Odaka, S. Iwata, N. Taga, S. Ohnishi, Y. Kaneta, and Y. Shigesato, Jpn. J. Appl. Phys. **36**, 5551 (1997).
[26] Y. Ohhata, F. Shinoki, and S. Yoshida, Thin Solid Films **59**, 255 (1979).
[27] F. Matino, L. Persano, V. Arima, D. Pisignano, R. I. R. Blyth, R. Cingolani, and R. Rinaldi, Phys. Rev. B **72**, 085437 (2005).
[28] C. Ambrosch-Draxl and J. O. Sofo, Comput. Phys. Commun. **175**, 1 (2006).
[29] P. Prathap, Y. P. V. Subbaiah, M. Devika, and K. T. Ramakrishna Reddy, Mater. Chem. Phys. **100**, 375 (2006).
[30] F. Fuchs and F. Bechstedt, Phys. Rev. B **77**, 155107 (2008).
[31] M. Cardona and G. Harbeke, Phys. Rev. **137**, A1468 (1965).
[32] I. Hamberg, C. G. Granqvist, K. F. Berggren, B. E. Sernelius, and L. Engström, Phys. Rev. B **30**, 3240 (1984).
[33] A. M. E. Raj, K. C. Lalithambika, V. S. Vidhya, G. Rajagopal, A. Thayumanavan, M. Jayachandran, and C. Sanjeeviraja, Physica B **403**, 544 (2008).
[34] W. W. Molzen, J. Vac. Sci. Technol. **12**, 99 (1975).
[35] H. Y. Valencia, L. C. Moreno, and A. M. Ardila, Microelectron. J. **39**, 1356 (2008).
[36] F. Wooten, Optical Properties of Solids (Academic Press, New York, 1972).
[37] H. R. Philipp and H. Ehrenreich, Phys. Rev. **129**, 1550 (1962).
[38] S. Loughin, R. H. French, L. K. Noyer, W.-Y. Ching, and Y.-N. Xu, J. Phys. D **29**, 1740 (1996).